This article has been accepted for publication in a future issue of this journal, but has not been fully edited. Content may change prior to final publication. Citation information: DOI 10.1109/TSG.2019.2912848, IEEE Transactions on Smart Grid

A Poverty Severity Index–Based Protection Strategy for Ring-Bus Low-Voltage DC Microgrids

Mehdi Salehi, Seyed Abbas Taher, *Senior Member, IEEE*, Iman Sadeghkhani, and Mohammad Shahidehpour, *Fellow, IEEE*

***Abstract*—The lack of an effective protection system may jeopardize resilience offered by low voltage DC (LVDC) microgrids. This paper presents a protection strategy for ring-bus LVDC microgrids, which employs intelligent electronic devices and solid-state circuit breakers (SSCBs). This scheme is developed based on monitoring the modified squared poverty gap index difference that is calculated using the normalized fault-imposed component of current. A backup protection scheme for the case of the SSCB failure and a reclosing scheme for restoring the isolated zone in the case of temporary faults are considered in the protection scheme. The proposed strategy is capable of detecting and classifying the pole-to-pole and pole-to-ground faults within microgrid lines. Moreover, it consists of protection schemes for distributed energy resource and load laterals and is effective for high-impedance fault detection. The merits of the developed protection strategy are demonstrated through several time-domain simulation case studies.**

***Index Terms*—Fault detection, directional protection, low voltage DC microgrid, squared poverty gap index, smart grid.**

I. Introduction

WITH increasing DC distributed energy resource (DER) units such as photovoltaics, energy storages, and fuel cells as well as modern DC consumers such as LEDs and sensitive computer loads, low-voltage DC (LVDC) microgrids are gaining great attention in the research community as an efficient energy component of future smart grids [1]–[3]. The main advantages of an LVDC microgrid are the reduction of multiple power conversion stages, lack of requirement for synchronization and frequency control, and elimination of reactive power and harmonic issues; such advantages turn the microgrid into a "back-to-Edison" phenomenon [4], [5]. The LVDC microgrid can be connected to the utility grid through the interlinking converter or may autonomously work to electrify remote areas such as rural power systems.

The lack of an effective protection scheme is one of the main challenges of LVDC microgrids due to the nature of DC faults [6]. Pole-to-pole (PP) and pole-to-ground (PG) are the various types of DC faults. The former fault occurs when two poles unintentionally connect together while the latter occurs when one pole comes in contact with the ground. The absence of natural zero crossing points, cables with low impedance, the presence of power electronic converters, fault currents with the high magnitude and rate of change, and need for fast DC circuit breakers make difficult the fault detection and clearance [6]–[8]. Thus, the design of a selective, sensitive, secure, and fast protection scheme is crucial to reduce the risk and cost of LVDC microgrids.

The proposed protective solutions in the literature can be categorized into two groups: (1) non-unit protection schemes and (2) unit protection schemes. In the latter protection schemes, the boundaries of the protection zone are clear while they are not for the former strategies. The non-unit protection scheme proposed in [9] uses the line current derivative. Ref. [10] protects the DC microgrid based on the natural characteristics of DC current and its first and second derivatives. A hybrid passive overcurrent relay is proposed in [6], employing the voltage and current transducers in addition to passive elements. By using the overcurrent function and real-time discrete wavelet transform, fault conditions with various fault resistances can be detected. The non-iterative fault location techniques using the probe power unit are proposed in [11], [12] for DC microgrids. Change in the magnitude and direction of fault current, as well as a rapid decrease in the DC voltage, are the basis of the protection solution presented in [13]. By injecting a short-duration spread frequency current, [14] measures the bus impedance to protect the DC marine power system. However, the non-unit protection schemes either present the proper sensitivity only for low-impedance faults detection or require the additional equipment. The low sensitivity may result in longer fault clearance time or disconnection of the larger section of the DC microgrid.

The second category schemes are proposed to enhance the sensitivity and speed of the DC protection system using the communication network. Developing the smart grid concept reduces the cost of unit protection schemes since its communication infrastructure can be used in such protection strategies [15]. By monitoring the magnitude of the differential current, [16] detects the fault conditions. Ref. [17] estimates the fault path parameter using the least square technique to determine the fault direction and distinguishes the internal faults from the external faults using the information of the fault direction at both ends of the protected line. The differential protection solutions based on the modified cumulative sum average approach are proposed in [18], [19] for bus-type DC microgrids. Ref. [20] detects a fault condition using oscillation frequency and determines the faulty section using the information of transient power at both ends. A directional current based protection scheme is proposed in [7], which makes the decision based on the information of the current direction at both ends of the protected zone.

M. Salehi and S. A. Taher are with the Department of Electrical Engineering, University of Kashan, Kashan 87317-51167, Iran (email: mehdi.salehi@grad.kashanu.ac.ir; sataher@kashanu.ac.ir).

I. Sadeghkhani is with the Smart Microgrid Research Center and the Department of Electrical Engineering, Najafabad Branch, Islamic Azad University, Najafabad 85141-43131, Iran (e-mail: sadeghkhani@pel.iaun.ac.ir).

M. Shahidehpour is with the Electrical and Computer Engineering Department, Illinois Institute of Technology, Chicago, USA (email: ms@iit.edu).

1949-3053 (c) 2018 IEEE. Personal use is permitted, but republication/redistribution requires IEEE permission. See http://www.ieee.org/publications_standards/publications/rights/index.html for more information.

This article has been accepted for publication in a future issue of this journal, but has not been fully edited. Content may change prior to final publication. Citation information: DOI 10.1109/TSG.2019.2912848, IEEE Transactions on Smart Grid

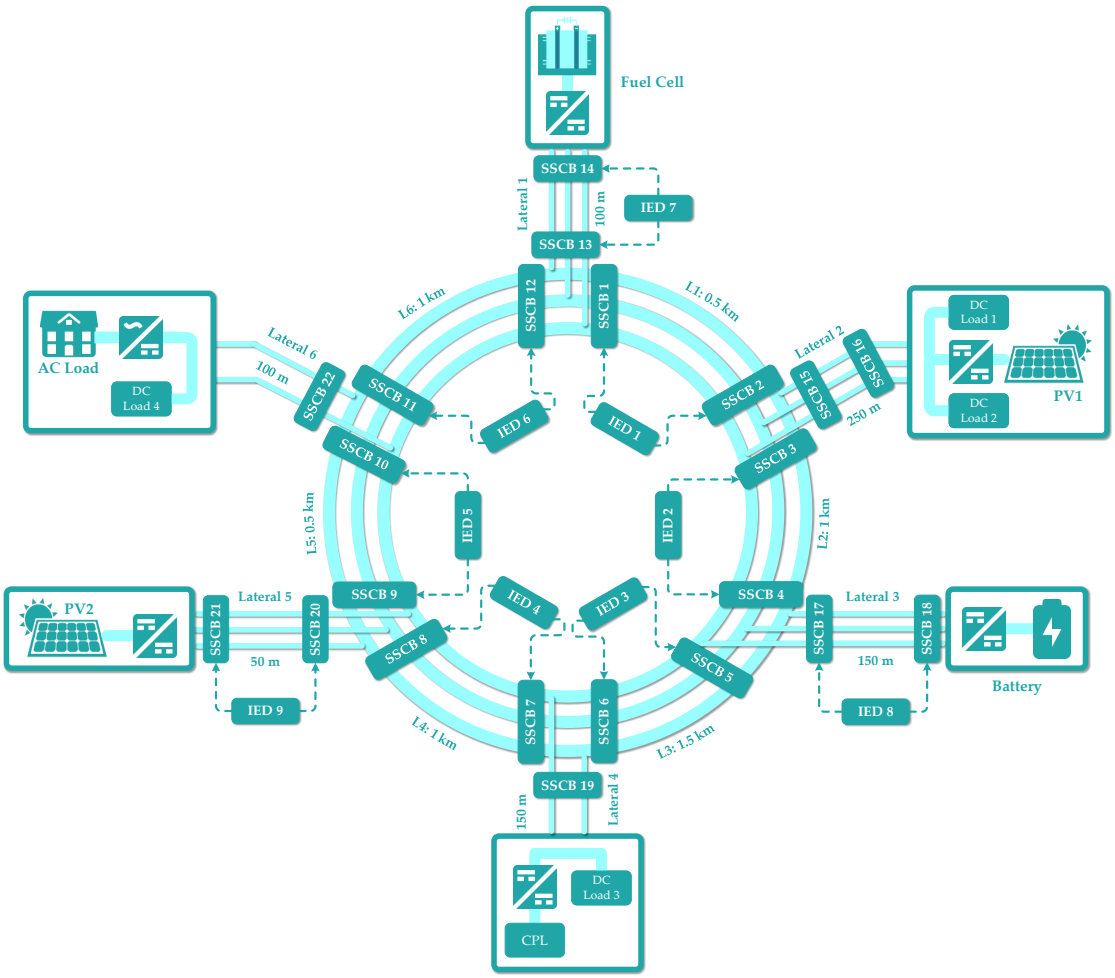

Fig. 1. Test ring-bus LVDC microgrid network.

One of the main challenges of a protection scheme is the detection of high-impedance faults (HIFs) since they do not significantly change the current/voltage magnitude. When a line falls on a high-impedance surface or comes in contact with a high-impedance object, an HIF occurs [21]. An HIF can be interpreted as a fault condition that cannot be able to change the direction of the fault current to be toward the fault location [6], [17] and consequently, the fault-imposed current is lower than the pre-fault current. This makes the directional protection ineffective. To solve this problem, [2], [22] employ the fault-imposed component of current and transient energy, respectively. However, the latter does not provide sufficient sensitivity for detecting HIFs and both methods do not develop a comprehensive protection scheme including the main protections, lateral protection, breaker failure protection, and reclosing scheme. To address these issues, this paper proposes a directional protection strategy for autonomous LVDC microgrids with ring configuration, which employs the current samples measured at both ends of the protected zone. Each zone is equipped with an intelligent electronic device (IED) that calculates the modified squared poverty gap index (MSPGI) to measure the severity of the fault condition using the fault-imposed component of current. To the best of our knowledge, it is the first time that this index is employed in power system studies. Based on MSPGI information from both ends, the faulty zone is determined. The proposed strategy includes a backup scheme for the event of switching device failure and a reclosing scheme for restoring the faulty zone in the case of temporary faults. Also, it is effective for HIFs. Specifically, the main features of this paper are as follows:

- It proposes a fault detection scheme with high sensitivity based on the MSPGI;
- It modifies the conventional directional protection using the MSPGI to protect the main ring bus;
- It develops protection schemes for protection of DGs interfaced using both unidirectional and bidirectional converters based on the MSPGI;
- It presents a reclosing scheme based on the MSPGI; and
- The proposed scheme is evaluated in an islanded LVDC microgrid.

The rest of the paper is organized as follows. The test ring-bus LVDC microgrid is introduced in Section II. Section III is dedicated to the proposed protection strategy, followed by the case studies in Section IV where the simulations are carried out to verify the effectiveness of the protection scheme. Finally, Section V concludes the paper.

1949-3053 (c) 2018 IEEE. Personal use is permitted, but republication/redistribution requires IEEE permission. See http://www.ieee.org/publications_standards/publications/rights/index.html for more information.

This article has been accepted for publication in a future issue of this journal, but has not been fully edited. Content may change prior to final publication. Citation information: DOI 10.1109/TSG.2019.2912848, IEEE Transactions on Smart Grid

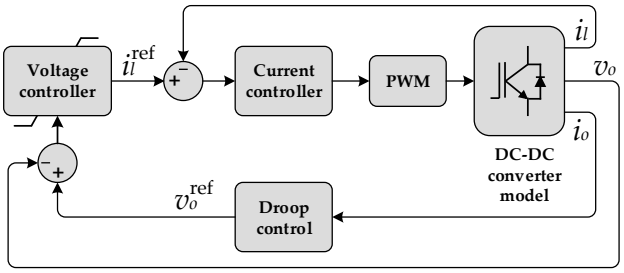

Fig. 2. Basic structure of DC-DC converter control.

II. LVDC Microgrid Test Model

Fig. 1 shows the study autonomous ring-bus LVDC microgrid. The operating DC voltage (selected as base voltage) and base power are chosen to be 350 V and 50 kW, respectively. The study microgrid is a 3-wire DC system (bipolar) with the grounding scheme of TN-S, where the middle point is grounded at each converter station. This grounding scheme is recommended by IEC for operating voltage up to 400 V DC pole-to-pole to provide proper safety margin [23]. Two photovoltaic (PV) arrays, one fuel cell (FC) stack, and one battery energize the autonomous LVDC microgrid. Moreover, there are several load types: four constant impedance loads, DC loads 1-4, one constant power load interfaced through a DC-DC converter, and one AC load interfaced through a DC-AC inverter. The study LVDC microgrid consists of 6 line segments, L1-L6, and 6 laterals, with the cross-section area of 240 mm^2, an aluminum conductor, PVC type-A insulation and PVC type ST-1 sheathing [24]. The test system data are given in Table I.

PV arrays and FC stack are interfaced through the unidirectional DC-DC boost converter while the battery is interfaced through a bidirectional DC-DC converter. PV1 is a grid following source and its DC-DC converter is controlled by perturb and observe maximum power point tracking (MPPT) algorithm, injecting the PV rated power to the microgrid. However, PV2, FC, and battery operate as the grid forming sources and their converters are controlled using the droop control [25] to reduce the circulating current among them. Fig. 2 shows the control system of DC-DC converters of study LVDC grid. The voltage reference v_o^{ref} made by the droop control is tracked by the voltage and current control loops. To protect the semiconductor switches from the severe overcurrent conditions, the current reference of the grid forming converters i_l^{ref} is limited to two times the rated current [26], [27].

TABLE I
Study LVDC Microgrid Parameters

Parameter	Value
System voltage	350 Vdc
Base power	50 kW
PV module	305.2 W, $V_{\text{mpp}} = 54.7$ V, $I_{\text{mpp}} = 5.58$ A at STC
PV1 and PV2 converter	15 kW
FC stack	45 V, 6 kW
Battery	96 V, 0.4 kAh
Battery converter	12 kW
DC loads 1-4	12.25, 5, 10.2, 12.25 kW
Constant power load	5 kW
AC load	3ϕ, $P = 6$ kW, $Q = 4$ kVAr
Filter Parameters	
PV converter filter	0.1 mF, 5 mH, 7.5 mF
FC converter filter	8 mH, 7.5 mF
Battery converter filter	1.2 mF, 1 mH, 130 mF
AC load filter	25 mH, 0.1 mF
DC link capacitor of AC load	25 mF
Control Parameters	
DC voltage controller proportional term	0.025
DC voltage controller integral term	0.3
DC current controller proportional term	0.025
DC current controller integral term	0.3
Droop coefficient of PV2, battery, FC stack	0.6, 0.75, 1.5
AC load voltage controller proportional term	10
AC load voltage controller integral term	300
AC load current controller proportional term	100
AC load current controller integral term	3000
Line Parameters	
Cross sectional area	240 mm^2
Cable resistance	0.125 Ω/km
Cable inductance	0.232 mH/km
Length of lines 1-6	0.5, 1, 1.5, 1, 0.5, 1 km
Length of laterals 1-6	100, 250, 150, 150, 50, 100 m

III. Proposed Protection Strategy

The bidirectional current flow in non-radial LVDC microgrids degrades the performance of directional element-less protection strategies. On the other hand, no change in current direction and no significant change in current amplitude during HIFs degrade the performance of directional protection schemes. To address the issue, this paper proposes a directional protection strategy that employs the information of current at both ends of the protected zone. In the first step, the fault-imposed component of current is calculated to overcome the problem of no change in current direction during HIFs. This component is zero during normal condition; however, it changes when a disturbance occurs. To overcome the problem of no significant change in current magnitude during HIFs, this paper proposes to use the MSPGI. By monitoring the MSPGI difference in a moving data window, the proposed scheme properly determines the faulty zone. The proposed protection strategy is described as follows.

A. Modified Squared Poverty Gap Index

The squared poverty gap index (SPGI), also known as the poverty severity index, was proposed to measure the severity of poverty for a certain population [28]. It takes into account the inequality among the poor. Unlike the poverty gap index, the SPGI specifies the weight based on the poverty gap and puts more weight on populations that fall well below the poverty line. This paper adopts this index to measure the severity of change in current samples during a disturbance. First, the line current i is measured using a current transducer and passed through a low-pass filter (LPF) to mitigate the noise. Using an IED, the current is sampled at 5 kHz. Then, it is normalized to enhance the scalability of the proposed scheme as

$$i^{\text{pu}}(kT_s) = \frac{i(kT_s)}{I_{\text{base}}}, \tag{1}$$

where k and T_s are the sampling step and sampling period,

1949-3053 (c) 2018 IEEE. Personal use is permitted, but republication/redistribution requires IEEE permission. See http://www.ieee.org/publications_standards/publications/rights/index.html for more information.

This article has been accepted for publication in a future issue of this journal, but has not been fully edited. Content may change prior to final publication. Citation information: DOI 10.1109/TSG.2019.2912848, IEEE Transactions on Smart Grid

respectively, and

$$I_{\text{base}} = \frac{P_{\text{base}}}{V_{\text{base}}}, \tag{2}$$

where I_{base}, V_{base}, and P_{base} are the base values of current, voltage, and power, respectively. Based on the superposition theorem, the current variable can be considered to consist of normal-running and fault-imposed components [29]. The latter has the signature of fault and is independent of the former. Consequently, one can write

$$i_{\text{FI}}^{\text{pu}}(kT_s) = i_{\text{F}}^{\text{pu}}(kT_s) - i_{\text{N}}^{\text{pu}}(kT_s), \tag{3}$$

where $i_{\text{FI}}^{\text{pu}}$, i_{F}^{pu}, and i_{N}^{pu} are the fault-imposed current, fault current, and normal condition current, respectively. Using the Delta filter [30], the fault-imposed current can be calculated as

$$i_{\text{FI}}^{\text{pu}}(kT_s) = i^{\text{pu}}(kT_s) - i^{\text{pu}}(kT_s - T_d), \tag{4}$$

where T_d is the time delay of the Delta filter.

The fault-imposed current is monitored in a moving data window, as shown in Fig. 3. The poverty gap G_j for the jth current sample is calculated as

$$G_j = \left(z - i_{\text{FI},j}^{\text{pu}}\right) \times u\left(z - i_{\text{FI},j}^{\text{pu}}\right), \tag{5}$$

where z is the poverty line and $u(.)$ is the unit step function. G_j indicates that how much the current sample $i_{\text{FI},j}^{\text{pu}}$ is less than the poverty line. For current samples greater than z, G_j is zero. Since the current increases during a fault condition, the poverty gap definition should be modified to measure the severity of current samples risen up to the poverty line. The modified poverty gap G'_j is expressed as

$$G'_j = \left(i_{\text{FI},j}^{\text{pu}} - z\right) \times u\left(i_{\text{FI},j}^{\text{pu}} - z\right), \tag{6}$$

During normal operation, $i_{\text{FI},j}^{\text{pu}}$ is zero; while when a fault occurs, it increases instantaneously. This increment increases the distance to the poverty line (G'_j). It should be noted that z is not zero due to measurement uncertainty. The modified squared poverty gap index is defined as

$$\begin{aligned}\text{MSPGI} &= \frac{1}{N}\sum_{j=1}^{N}\left(\frac{G'_j}{z}\right)^2 \\ &= \frac{1}{N}\sum_{j=1}^{N}\left(\frac{\left(i_{\text{FI},j}^{\text{pu}} - z\right) \times u\left(i_{\text{FI},j}^{\text{pu}} - z\right)}{z}\right)^2,\end{aligned} \tag{7}$$

where N is the length of the moving data window.

The MSPGI quantifies the severity of a change in current in two stages as follows.

1) Triggering: The presence of noise in the measurements and normal variations of LVDC microgrid current due to weather disturbance and connection/disconnection of loads result in the fault-imposed current is not exactly zero during the normal operation. To reduce the computational burden and to prevent the mal-operation of the protection system, MSPGI is calculated for those current samples that are above the threshold (poverty line z).

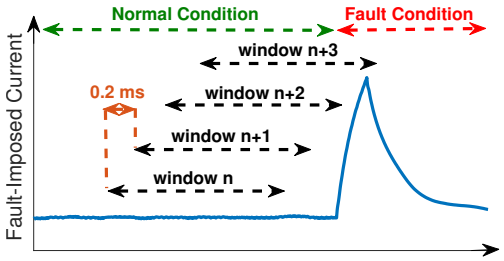

Fig. 3. The fault-imposed current for a typical fault condition and the moving windows.

2) Weighting: To quantify the severity of a change in current, MSPGI takes into account inequality among the current samples. This index is a weighted sum of poverty gaps (as a proportion of the poverty line), where the weights are the proportionate poverty gaps themselves. The weighting process consists of two steps. First, the current samples are divided by the poverty line (which is a small value in perunit) to quantify their distance to the poverty line. Then, the resultant is squared to magnify the change in current during the fault condition.

B. Line Protection

This paper proposes to use the directional protection strategy for protection of microgrid lines, as shown in Fig. 4(a). To interrupt the DC current, each line is equipped with two solid state circuit breakers (SSCBs) that can operate within few microseconds (50 μs delay is typical) [10], [13]. The IED installed for each line receives the information of current for both ends and calculates the MSPGI at each end. Using a fiber optic with high bandwidth and advanced routing, and given the short lines of LVDC microgrids, the total communication delays including transmission delay, propagation delay, queuing delay, and processing delay can be about 0.1 ms [7]. The proposed directional protection principle is expressed as

$$\Delta\text{MSPGI} = \left|\text{MSPGI}_{\text{S}} - \text{MSPGI}_{\text{R}}\right|, \tag{8}$$

where MSPGI_{S} and MSPGI_{R} are the calculated MSPGI for sending and receiving ends, respectively. ΔMSPGI is the MSPGI difference. When the ΔMSPGI exceeds the fault detection threshold ε, the disturbance is detected and the process of faulty line identification is started.

In the case of a forward external fault (Fig. 4b), the measured currents at both ends of the protected zone are

$$i_{\text{F,S}}^{\text{pu}} = i_{\text{N,S}}^{\text{pu}} + i_f^{\text{pu}}, \tag{9}$$

$$i_{\text{F,R}}^{\text{pu}} = i_{\text{N,R}}^{\text{pu}} + i_f^{\text{pu}}, \tag{10}$$

where $i_{\text{F,S}}^{\text{pu}}$ and $i_{\text{F,R}}^{\text{pu}}$ are the sending and receiving end fault currents; $i_{\text{N,S}}^{\text{pu}}$ and $i_{\text{N,R}}^{\text{pu}}$ are the sending and receiving end normal condition currents, respectively; and i_f^{pu} is the fault current. The fault-imposed components of currents are

$$i_{\text{FI,S}}^{\text{pu}} = i_{\text{FI,R}}^{\text{pu}} = i_f^{\text{pu}}. \tag{11}$$

In this condition, MSPGI_{S} is equal to MSPGI_{R} and consequently, the ΔMSPGI is zero.

In the case of the reverse external fault (Fig. 4c), the currents at both ends of the protected line are

$$i_{\text{F,S}}^{\text{pu}} = i_{\text{N,S}}^{\text{pu}} - i_f^{\text{pu}}, \tag{12}$$

$$i_{\text{F,R}}^{\text{pu}} = i_{\text{N,R}}^{\text{pu}} - i_f^{\text{pu}}, \tag{13}$$

1949-3053 (c) 2018 IEEE. Personal use is permitted, but republication/redistribution requires IEEE permission. See http://www.ieee.org/publications_standards/publications/rights/index.html for more information.

This article has been accepted for publication in a future issue of this journal, but has not been fully edited. Content may change prior to final publication. Citation information: DOI 10.1109/TSG.2019.2912848, IEEE Transactions on Smart Grid

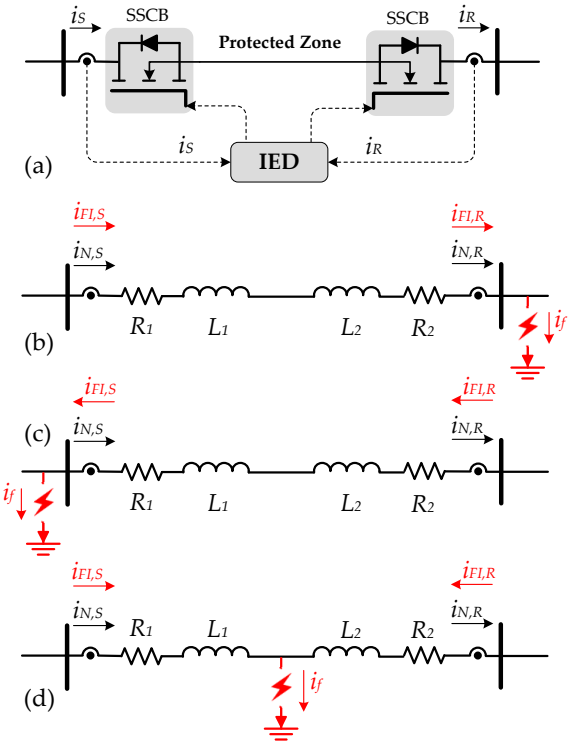

Fig. 4. (a) The proposed line protection scheme, (b) line model for the forward external fault, (c) line model for the reverse external fault, and (d) line model for the internal fault.

Thus, the fault-imposed currents are expressed as

$$i^{\mathrm{pu}}_{\mathrm{FI,S}} = i^{\mathrm{pu}}_{\mathrm{FI,R}} = -i^{\mathrm{pu}}_{f}. \tag{14}$$

Since the fault-imposed currents are negative, the samples at both ends fall below the poverty line and consequently, $\mathrm{MSPGI_S} = \mathrm{MSPGI_R} = 0$. Thus, the ΔMSPGI becomes zero.

Fig. 4(d) shows that when a fault occurs within the protected zone, the normal condition and fault-imposed currents at sending end and receiving end are in the same direction and in the opposite direction, respectively. Consequently,

$$i^{\mathrm{pu}}_{\mathrm{FI,S}} = i^{\mathrm{pu}}_{\mathrm{F,S}} - i^{\mathrm{pu}}_{\mathrm{N,S}} > 0, \tag{15}$$

$$i^{\mathrm{pu}}_{\mathrm{FI,R}} = i^{\mathrm{pu}}_{\mathrm{F,R}} - i^{\mathrm{pu}}_{\mathrm{N,R}} < 0. \tag{16}$$

The positive fault-imposed current samples lead to a positive MSPGI for the sending end while the negative fault-imposed current samples result in zero MSPGI for the receiving end; consequently, the $\Delta\mathrm{MSPGI} \neq 0$. In this condition, the fault is identified as an internal fault and the IED commands both SSCBs to isolate the protected line.

The ΔMSPGI is calculated for currents of positive and negative poles. If both $\Delta\mathrm{MSPGI}^{+}$ and $\Delta\mathrm{MSPGI}^{-}$ are positive, the fault is a PP fault. If only $\Delta\mathrm{MSPGI}^{+}$ is positive and the $\Delta\mathrm{MSPGI}^{-}$ is zero, the fault is classified as a PG fault.

C. SSCB Failure

When the fault condition is detected and the opening command is sent to the SSCBs of the faulty zone, the IED monitors the action of these switching devices. If sending and/or receiving end currents are still non-zero, the SSCB failed to de-energize the line. In this condition, the faulty zone IED sends a backup signal to the adjacent zone IED(s) after a certain time delay. The adjacent zone IED sends the tripping command to the SSCB located on the same bus of the failed SSCB to improve the system reliability.

D. Reclosing Scheme

Most of the fault conditions are temporary events caused by the animals, tree branches, lightning, and so on [11]. Thus, a reclosing scheme can speed up the restoration of the faulty zone. After a certain time delay, the faulty zone IED sends the closing command to the SSCBs of both ends. If the ΔMSPGI is non-zero, the fault persists and the opening command is sent again to the SSCBs. Otherwise, the fault was cleared and the SSCBs remain closed. It should be noted that the number of reclosing attempts is limited to prevent the equipment damage.

E. Flowchart of Proposed Line Protection Algorithm

Fig. 5 shows the flowchart of the proposed MSPGI-based directional protection. The Fault Detection and Isolation section calculates the MSPGI for fault-imposed currents at both ends. Then, the MSPGI difference is calculated to determine the faulty zone. If the ΔMSPGI is greater than the fault detection threshold, the disturbance is an internal fault and the trip command is sent to the SCCBs by the IED. If the fault current persists, the Breaker Failure section notifies the adjacent IED(s) to trip the SCCB(s) on the same bus of the failed SCCB(s). The Reclosing Scheme section tries to restore the faulty zone by reclosing the SCCBs after a certain time delay. The reclosing attempt is repeated until its maximum allowable number is reached. The Fault Classification section determines the type of fault. If the ΔMSPGI is zero, there is no fault or the fault is an external fault while a non-zero value for the ΔMSPGI indicates an internal fault. In the case of internal faults, the ΔMSPGI is calculated for both positive and negative poles. The positive values for the $\Delta\mathrm{MSPGI}^{+}$ and $\Delta\mathrm{MSPGI}^{-}$ indicate a PP fault while zero value for the $\Delta\mathrm{MSPGI}^{-}$ indicates a PG fault.

F. Lateral Protection

If a lateral includes only DER units, or its power generation is greater than its power consumption, the proposed MSPGI is employed to protect the lateral against fault conditions. In the case of the PV array and FC stack, the proposed non-unit protection is shown in Fig. 6(a). In this case, the current is measured at network side end of lateral in opposite direction with the DER injected current. Thus, during normal operation, the measured current is negative. When a fault occurs within the lateral, both the DER and microgrid inject the fault current to the lateral. In this condition, the measured current is the fault current flowing from the LVDC microgrid and is positive. Thus, the fault-imposed current is

$$i^{\mathrm{pu}}_{\mathrm{FI}} = i^{\mathrm{pu}}_{f,\mathrm{MG}} - (-i^{\mathrm{pu}}_{\mathrm{DER}}) > 0, \tag{17}$$

where $i^{\mathrm{pu}}_{\mathrm{DER}}$ is the DER injected current in the normal condition and $i^{\mathrm{pu}}_{f,\mathrm{MG}}$ is the fault current flowing from the LVDC microgrid; consequently, $\mathrm{MSPGI} \neq 0$ and the IED commands

1949-3053 (c) 2018 IEEE. Personal use is permitted, but republication/redistribution requires IEEE permission. See http://www.ieee.org/publications_standards/publications/rights/index.html for more information.

This article has been accepted for publication in a future issue of this journal, but has not been fully edited. Content may change prior to final publication. Citation information: DOI 10.1109/TSG.2019.2912848, IEEE Transactions on Smart Grid

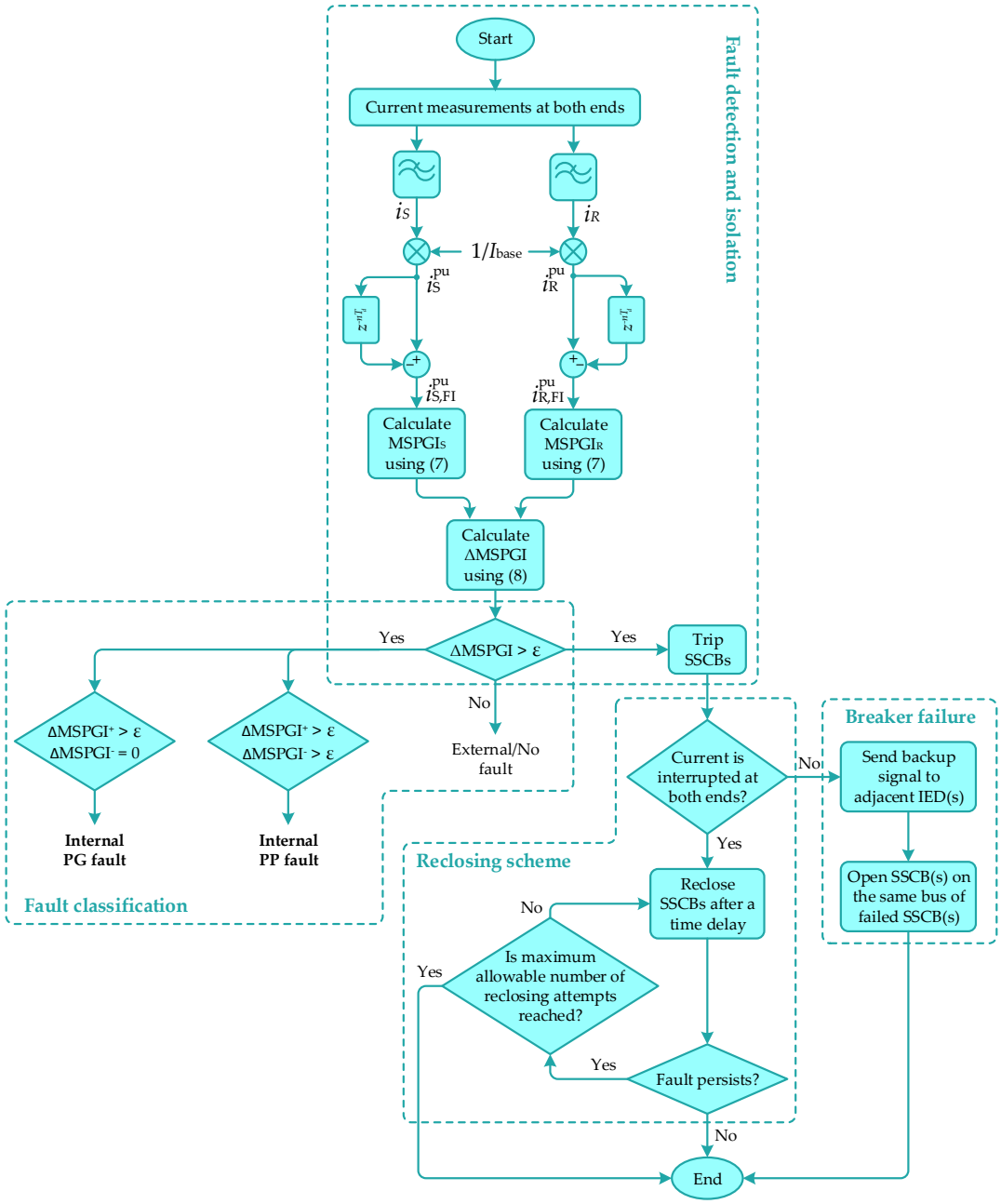

Fig. 5. Flowchart of the proposed directional line protection scheme.

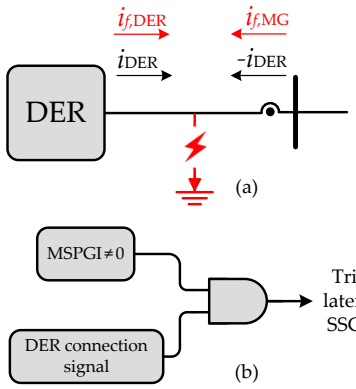

Fig. 6. (a) The current direction during the DER lateral fault; (b) the logic circuit for the PV and FC lateral protections.

the both SSCBs to interrupt the current. However, this protection scheme miss-operates when the DER is disconnected. It is due to this fact that when the lateral includes only the DER and it is disconnected, the post-disturbance current is zero and thus $i_{\mathrm{FI}}^{\mathrm{pu}} > 0$. Moreover, in the case of lateral with DER and loads, before DER disconnection, the loads are supplied by both the DER and DC microgrid; however, when the DER is disconnected, the loads are supplied only by the DC microgrid and consequently, the injected current by the DC microgrid increases. Thus, $i_{\mathrm{FI}}^{\mathrm{pu}} > 0$, and the $\mathrm{MSPGI} \neq 0$. To prevent the mal-operation of the protection system, the disconnected DER should send a signal to the IED for disabling the MSPGI calculation, as shown in Fig. 6(b).

On the other hand, since the battery employs a bidirectional

1949-3053 (c) 2018 IEEE. Personal use is permitted, but republication/redistribution requires IEEE permission. See http://www.ieee.org/publications_standards/publications/rights/index.html for more information.

This article has been accepted for publication in a future issue of this journal, but has not been fully edited. Content may change prior to final publication. Citation information: DOI 10.1109/TSG.2019.2912848, IEEE Transactions on Smart Grid

DC-DC converter and its lateral current flow is bidirectional, the MSPGI-based directional protection should be employed for battery lateral.

If a lateral does not include any DER, or its power consumption is greater than its power generation, the current direction is always from the DC microgrid to the lateral. In this condition, a simple current magnitude comparison method can be used. If the lateral current is greater than its full load current, the protection scheme isolates this lateral from the DC microgrid.

IV. Performance Evaluation

A set of simulation case studies is reported in this section to evaluate the proposed protection strategy. The case studies are performed on a simulation model of the LVDC microgrid in Fig. 1 using the MATLAB/Simulink environment. The developed scenarios are the PP fault, PG fault, fault in the lateral, and HIF. In addition, a comparison with the existing methods is presented. The length of the moving data window N, time delay of Delta filter T_d, poverty line z, and fault detection threshold ε is selected equal to 2, 0.1 s, 0.02 pu, and 0.1, respectively.

A. Case 1: Pole-to-Pole Fault

The first scenario is dedicated to investigating the performance of the proposed MSPGI-based directional protection scheme during PP faults. To this end, a PP fault is simulated in the middle of line 1 (L1 in Fig. 1). The fault resistance is 0.1 Ω and it is initiated at $t = 6$ s. Fig. 7 shows the simulation results for this case. Both the ΔMSPGI^+ and ΔMSPGI^- are plotted for all the line sections. The results show that the MSPGI difference has a non-zero value only for L1. The ΔMSPGI^+ increases to 1750 while the ΔMSPGI^- increases to 1534, both of which are well above the threshold. Since the ΔMSPGI for both the positive and negative poles is greater than the threshold, the disturbance is properly classified as a PP fault. The ΔMSPGI exceeds the threshold at $t = 6.001$ s. Considering the total communication and SCCB operating time delays of 200 μs, the fault detection time is about 1.2 ms. Table II shows the ΔMSPGI for PP faults with fault resistances of 0.1, 0.5, 2, and 15 Ω in all lines of the study LVDC microgrid. The results verify the sensitivity of the proposed protection scheme for detecting PP faults.

B. Case 2: Pole-to-Ground Fault

The second scenario evaluates the effectiveness of the proposed protection strategy during PG faults. In this case,

TABLE II
THE ΔMSPGI CALCULATED FOR VARIOUS PP FAULTS WITHIN THE TEST LVDC MICROGRID.

Fault Location	$\mathbf{R_f = 0.1\Omega}$	$\mathbf{R_f = 0.5\Omega}$	$\mathbf{R_f = 2\Omega}$	$\mathbf{R_f = 15\Omega}$
Line 1	2608	599.2	143.8	5.61
Line 2	3917	1725	508.5	23.7
Line 3	7992	3646	875.6	22.06
Line 4	8711	3618	799.4	17.88
Line 5	9665	3948	812.3	16.24
Line 6	2376	514.6	127	5.09

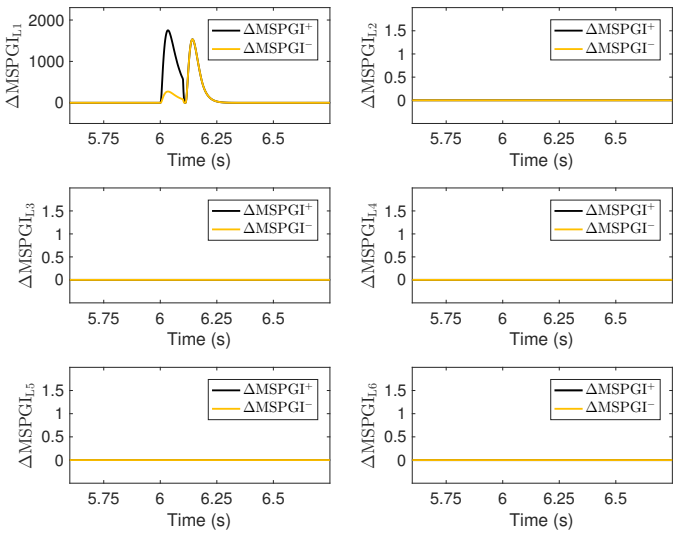

Fig. 7. The ΔMSPGI calculated for all lines of the test microgrid during a PP fault with fault resistance of 0.1 Ω.

a PG fault with fault resistance of 3 Ω is simulated in line 4 (L4 in Fig. 1) at $t = 6$ s. The calculated MSPGI difference for both the positive and negative poles in all lines is shown in Fig. 8. All the calculated ΔMSPGIs are lower than the threshold except those for L4. For this line, the ΔMSPGI^+ reaches 50.21 while the ΔMSPGI^- is zero; consequently, the disturbance is classified as a PG fault. Table III indicates the ability of the proposed scheme for detecting various PG fault conditions.

C. Case 3: Fault in Lateral

The objective of this scenario is to demonstrate the performance of the proposed protection scheme in the case of fault occurrence in the laterals. First, a PG fault is studied at the PV2 lateral. As mentioned in Subsection III.F, the protection of the PV and FC laterals is based on calculating the MSPGI and no difference based index is required. The fault is initiated at $t = 6$ s and the fault resistance is 0.5 Ω. Fig. 9(a) shows the calculated MSPGI for PV2 and FC laterals. The calculated

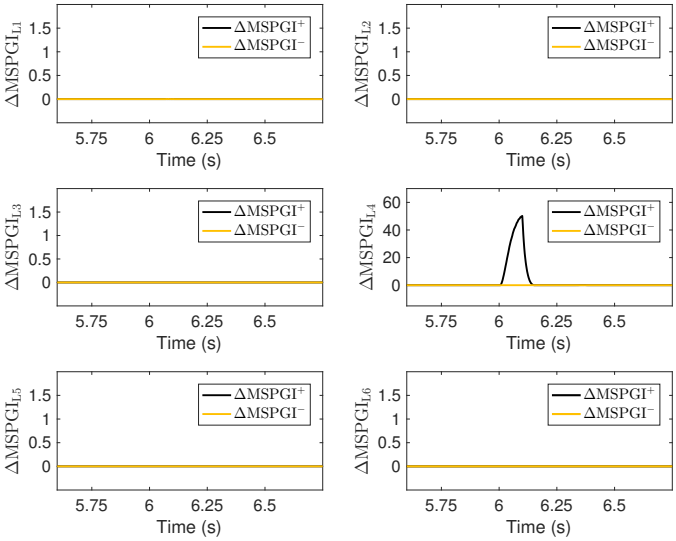

Fig. 8. The ΔMSPGI calculated for all lines of the test microgrid during a PG fault with fault resistance of 3 Ω.

1949-3053 (c) 2018 IEEE. Personal use is permitted, but republication/redistribution requires IEEE permission. See http://www.ieee.org/publications_standards/publications/rights/index.html for more information.

This article has been accepted for publication in a future issue of this journal, but has not been fully edited. Content may change prior to final publication. Citation information: DOI 10.1109/TSG.2019.2912848, IEEE Transactions on Smart Grid

TABLE III
THE ΔMSPGI CALCULATED FOR VARIOUS PG FAULTS WITHIN THE TEST LVDC MICROGRID.

Fault Location	$R_f = 0.1\Omega$	$R_f = 0.5\Omega$	$R_f = 2\Omega$	$R_f = 15\Omega$
Line 1	2460	260.5	25.84	0.41
Line 2	3552	499.1	107.5	3.14
Line 3	2825	1108	225.7	3.24
Line 4	3452	1205	212.5	2.47
Line 5	4203	1360	218.5	2.36
Line 6	1611	180.3	22.5	0.35

MSPGI for PV2 lateral increases to 2019 while it is zero for the FC stack lateral. Consequently, the fault is properly detected and the trip command is sent to the SSCB 20 and SSCB 21.

Next, the case of a PG fault at the AC load lateral is studied. The protection of load laterals is based on current magnitude comparison, as mentioned in Subsection III-F. The full load current for this lateral is the sum of the rated current of the AC load and DC load 4 and is equal to 26.1 A. A PP fault with fault resistance of 1.5 Ω is simulated in this lateral at $t = 6$ s. Fig. 9(b) shows the measured current at this lateral. The fault current increases to 81.8 A, which is greater than the full load current and consequently, the trip command is sent to the SSCB 22.

D. Case 4: Comparative Assessment

This case study is dedicated to evaluating the performance of the proposed protection strategy in comparison with current- and transient energy-based difference protections for DC microgrids in the case of HIFs. For this purpose, three PG HIFs with fault resistances of 20, 25, and 30 Ω are simulated at the middle of line 2 (L2 in Fig. 1). Fig. 10 shows the simulation results. The differential current Δi increases only to 5%, 4%, and 3%, respectively, that cannot be detected by the differential

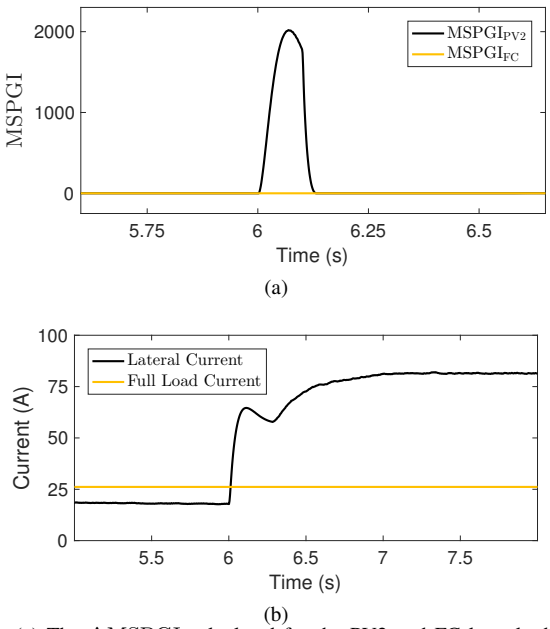

Fig. 9. (a) The ΔMSPGI calculated for the PV2 and FC laterals during a PG fault with $R_f = 0.5\,\Omega$ at the PV2 lateral; (b) Current magnitude of the AC load lateral during a PP fault with fault resistance of 1.5 Ω at that lateral.

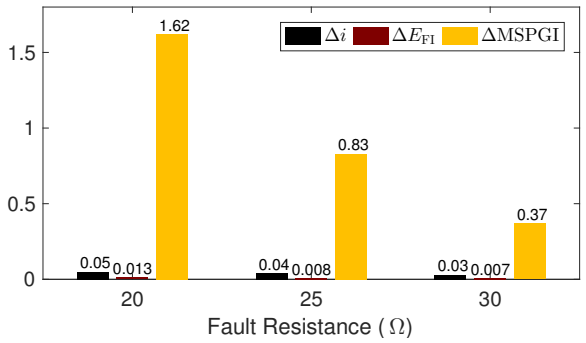

Fig. 10. Comparison between the performance of the proposed MSPGI-based protection strategy and current- and transient energy-based difference protection schemes.

relay since they are below the differential relay threshold of 10%. Also, the transient energy difference ΔE_{FI} [22] increases only to 1.3%, 0.8%, and 0.7%, respectively; these low values may not be detected because reducing the detection threshold may result in nuisance tripping. However, the proposed ΔMSPGI reaches 162%, 83%, and 37%, respectively, that are well above the fault detection threshold of 10%, verifying the high sensitivity of the proposed protection strategy. It should be noted that the two-level filtering using LPFs and Triggering stage minimizes the effect of noisy measurements on the performance of the proposed protection strategy in the case of HIFs.

V. CONCLUSION

This paper is motivated by the lack of a sensitive and comprehensive protection scheme for LVDC microgrids with ring configuration. The developed protection scheme is based on the directional protection principle. Calculating the fault-imposed current tackles the problem of no change in the current direction during low fault current cases while employing the modified squared poverty gap index difference enhances the sensitivity of the protection system during HIFs. The proposed scheme consists of one IED for each protected zone, which is capable of detecting the fault condition and communicating with adjacent IEDs in the event of switching device failure. Moreover, it includes a reclosing scheme to restore the faulty zone in the case of temporary faults. The protection of battery lateral is based on the ΔMSPGI-based directional protection while PV and FC laterals are protected by monitoring the MSPGI at network side end. Additionally, a current magnitude comparison scheme is employed to protect the load lateral. Several PP, PG, and HIF scenarios performed on the test ring-bus islanded LVDC microgrid verify the promising performance of the proposed protection strategy.

REFERENCES

[1] Z. Li and M. Shahidehpour, "Small-signal modeling and stability analysis of hybrid AC/DC microgrids," *IEEE Trans. Smart Grid*, vol. 10, no. 2, pp. 2080–2095, Mar. 2019.
[2] R. Mohanty and A. K. Pradhan, "A superimposed current based unit protection scheme for DC microgrid," *IEEE Trans. Smart Grid*, vol. 9, no. 4, pp. 3917–3919, Jul. 2018.
[3] S. Mudaliyar and S. Mishra, "Coordinated voltage control of a grid connected ring DC microgrid with energy hub," *IEEE Trans. Smart Grid*, vol. 10, no. 2, pp. 1939–1948, Mar. 2019.

1949-3053 (c) 2018 IEEE. Personal use is permitted, but republication/redistribution requires IEEE permission. See http://www.ieee.org/publications_standards/publications/rights/index.html for more information.

This article has been accepted for publication in a future issue of this journal, but has not been fully edited. Content may change prior to final publication. Citation information: DOI 10.1109/TSG.2019.2912848, IEEE Transactions on Smart Grid

[4] P. Prabhakaran, Y. Goyal, and V. Agarwal, "A novel communication-based average voltage regulation scheme for a droop controlled DC microgrid," *IEEE Trans. Smart Grid*, vol. 10, no. 2, pp. 1250–1258, Mar. 2019.

[5] J. M. Guerrero, A. Davoudi, F. Aminifar, J. Jatskevich, and H. Kakigano, "Guest editorial: Special section on smart DC distribution systems," *IEEE Trans. Smart Grid*, vol. 5, no. 5, pp. 2473–2475, Sept. 2014.

[6] K. A. Saleh, A. Hooshyar, and E. F. El-Saadany, "Hybrid passive-overcurrent relay for detection of faults in low-voltage DC grids," *IEEE Trans. Smart Grid*, vol. 8, no. 3, pp. 1129–1138, May 2017.

[7] A. A. S. Emhemed, K. Fong, S. Fletcher, and G. M. Burt, "Validation of fast and selective protection scheme for an LVDC distribution network," *IEEE Trans. Power Del.*, vol. 32, no. 3, pp. 1432–1440, Jun. 2017.

[8] S. D. A. Fletcher, P. J. Norman, S. J. Galloway, and G. M. Burt, "Analysis of the effectiveness of non-unit protection methods within DC microgrids," in *IET Conference on Renewable Power Generation*, Sept. 2011.

[9] A. Meghwani, S. C. Srivastava, and S. Chakrabarti, "A new protection scheme for DC microgrid using line current derivative," in *IEEE Power Energy Society General Meeting*, Jul. 2015.

[10] ——, "A non-unit protection scheme for DC microgrid based on local measurements," *IEEE Trans. Power Del.*, vol. 32, no. 1, pp. 172–181, Feb. 2017.

[11] J. D. Park, J. Candelaria, L. Ma, and K. Dunn, "DC ring-bus microgrid fault protection and identification of fault location," *IEEE Trans. Power Del.*, vol. 28, no. 4, pp. 2574–2584, Oct. 2013.

[12] R. Mohanty, U. S. M. Balaji, and A. K. Pradhan, "An accurate non-iterative fault-location technique for low-voltage DC microgrid," *IEEE Trans. Power Del.*, vol. 31, no. 2, pp. 475–481, Apr. 2016.

[13] A. A. S. Emhemed and G. M. Burt, "An advanced protection scheme for enabling an LVDC last mile distribution network," *IEEE Trans. Smart Grid*, vol. 5, no. 5, pp. 2602–2609, Sept. 2014.

[14] E. Christopher, M. Sumner, D. Thomas, X. Wang, and d. W. Frans, "Fault location in a zonal DC marine power system using active impedance estimation," in *IEEE Energy Conversion Congress and Exposition*, Sept. 2010, pp. 3050–3054.

[15] S. D. A. Fletcher, P. J. Norman, S. J. Galloway, P. Crolla, and G. M. Burt, "Optimizing the roles of unit and non-unit protection methods within DC microgrids," *IEEE Trans. Smart Grid*, vol. 3, no. 4, pp. 2079–2087, Dec. 2012.

[16] S. D. A. Fletcher, P. J. Norman, K. Fong, S. J. Galloway, and G. M. Burt, "High-speed differential protection for smart DC distribution systems," *IEEE Trans. Smart Grid*, vol. 5, no. 5, pp. 2610–2617, Sept. 2014.

[17] R. Mohanty and A. K. Pradhan, "Protection of smart DC microgrid with ring configuration using parameter estimation approach," *IEEE Trans. Smart Grid*, vol. 9, no. 6, pp. 6328–6337, Nov. 2018.

[18] S. Dhar, R. K. Patnaik, and P. K. Dash, "Fault detection and location of photovoltaic based DC microgrid using differential protection strategy," *IEEE Trans. Smart Grid*, vol. 9, no. 5, pp. 4303–4312, Sep. 2018.

[19] S. Dhar and P. K. Dash, "Differential current-based fault protection with adaptive threshold for multiple PV-based DC microgrid," *IET Renew. Power Gen.*, vol. 11, no. 6, pp. 778–790, 2017.

[20] R. Mohanty and A. K. Pradhan, "DC ring bus microgrid protection using the oscillation frequency and transient power," *IEEE Syst. J.*, vol. 13, no. 1, pp. 875–884, Mar. 2019.

[21] B. Fani, H. Bisheh, and I. Sadeghkhani, "Protection coordination scheme for distribution networks with high penetration of photovoltaic generators," *IET Gener. Transm. Distrib.*, vol. 12, no. 8, pp. 1802–1814, 2018.

[22] R. Mohanty and A. K. Pradhan, "Protection of DC and hybrid AC-DC microgrids with ring configuration," in *7th International Conference on Power Systems*, Pune, India, Dec. 2017.

[23] "DC distribution system and consequences for RCDs," The IEC 23E/WG2 workshop.

[24] "LT/HT power & control cables," [Online]. Available: https://www.havells.com/content/dam/havells/brouchers/Industrial Cable/Cable Catalogue-2016.pdf.

[25] J. M. Guerrero, J. C. Vasquez, J. Matas, L. G. de Vicuna, and M. Castilla, "Hierarchical control of droop-controlled AC and DC microgrids—A general approach toward standardization," *IEEE Trans. Ind. Electron.*, vol. 58, no. 1, pp. 158–172, Jan. 2011.

[26] G. C. Konstantopoulos and Q. Zhong, "Current-limiting DC/DC power converters," *IEEE T. Contr. Syst. T.*, vol. 27, no. 2, pp. 855–863, Mar. 2019.

[27] I. Sadeghkhani, M. E. H. Golshan, J. M. Guerrero, and A. Mehrizi-Sani, "A current limiting strategy to improve fault ride-through of inverter interfaced autonomous microgrids," *IEEE Trans. Smart Grid*, vol. 8, no. 5, pp. 2138–2148, Sept. 2017.

[28] W. B. Institute, "Introduction to poverty analysis," http://siteresources.worldbank.org/PGLP/Resources/PovertyManual.pdf, Tech. Rep., 2005.

[29] M. A. Zamani, A. Yazdani, and T. S. Sidhu, "A communication-assisted protection strategy for inverter-based medium-voltage microgrids," *IEEE Trans. Smart Grid*, vol. 3, no. 4, pp. 2088–2099, Dec. 2012.

[30] G. Benmouy and J. Roberts, "Superimposed quantities: Their true nature and application in relays, schweitzer engineering laboratories," *Inc. Pullman, WA USA, SEL USA*, 1999.

Mehdi Salehi was born in Isfahan, Iran, in 1993. He received the B.Sc. (Hons.) degree in electrical engineering from Najafabad Branch, Islamic Azad University, Najafabad, Iran, in 2016, and the M.Sc. (Hons.) degree in electrical engineering from University of Kashan, Kashan, Iran, in 2018. His major research interests include protection of microgrids, renewable energy sources, control of electronically-coupled distributed generation units, and smart grids.

Seyed Abbas Taher (SM'17) was born in Kashan, Isfahan, Iran, in 1964. He received his B.Sc. degree in electrical engineering from the Amirkabir University of Technology, Tehran, Iran, in 1988, and his M.Sc. and Ph.D. degrees in electrical engineering from the Tarbiat Modares University, Tehran, Iran, in 1991 and 1997, respectively. In 1996, he joined the faculty of engineering, University of Kashan, where he has been a Full Professor since 2016. His current research interests include power system optimization and control design, analysis of electrical machines, power quality, and renewable energy.

Iman Sadeghkhani received the Ph.D. degree in electrical engineering from the Isfahan University of Technology, Isfahan, Iran, in 2017. He is currently an Assistant Professor at Najafabad Branch, Islamic Azad University, Najafabad, Iran. His areas of interest include protection and control of both AC and DC microgrids and electronically interfaced distributed energy resources. Dr. Sadeghkhani was a recipient of the University of Kashan Award for Distinguished Research in 2010 and the Exceptional Reviewer Award from the IEEE TRANSACTIONS ON POWER DELIVERY in 2014.

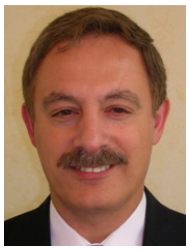

Mohammad Shahidehpour (F'01) received the Honorary Doctorate degree from the Polytechnic University of Bucharest, Bucharest, Romania. He is a University Distinguished Professor, Bodine Chair Professor, and Director of the Robert W. Galvin Center for Electricity Innovation at Illinois Institute of Technology, Chicago, IL, USA. He is a member of the US National Academy of Engineering, Fellow of IEEE, Fellow of the American Association for the Advancement of Science (AAAS), and Fellow of the National Academy of Inventors (NAI). Dr. Shahidehpour was a recipient of the IEEE PES Outstanding Power Engineering Educator Award.

1949-3053 (c) 2018 IEEE. Personal use is permitted, but republication/redistribution requires IEEE permission. See http://www.ieee.org/publications_standards/publications/rights/index.html for more information.